# ECE Radiometry in the TCABR Tokamak

R. P. da Silva, A. M. M. Fonseca, J. H. Vuolo, E. R. Calderon, R. M. O. Galvão,
Yu. K. Kuznetzov, J. C. Raffaelli*, and the TCABR Team
*Instituto de Física, Universidade de São Paulo, 05315-970, São Paulo, Brazil*

Received on 04 February, 2004; revised version received on 10 May, 2004

A millimeter/microwave detection system, in operation in the TCABR Tokamak is described. The system is used for electron cyclotron measurements. The main part of the system is a heterodyne sweeping radiometer based on a $BWO$ oscillator that operates in the frequency range of 52 to 85 $GHz$. The system operates in two modes : fixed frequency ( maximum resolution of 10 $\mu s$ ) and sweeping mode ( 50 $\mu s$ per frequency step ). The radiometer is calibrated in frequency and in radiation intensity. The frequency calibration is made by means of a precision harmonic oscillator. The absolute calibration was done using a blackbody ( microwave absorber ) immersed in liquid nitrogen ( 77 $K$ ) and also put in an oven with adjustable temperature up to $1470\,K$. Two others components are also used for periodic intensity calibration check and sensibility measurements : a Criogenic Matched Load and a Noise Source. A Gaussian antenna is used for better space resolution measurements. Between the antenna and the radiometer, oversized waveguides are used to reduced the signal attenuation. The antenna axis is in the equatorial plane of the machine and perpendicular to the plasma column axis. The accessibility and absorption conditions are discussed. Results showing time and radial profiles of the detected $ECE$ radiation for the TCABR are presented. For a magnetic field of $B_{TO} = 1.14\,T$ it was verified that the maximum permissible density to access the second harmonic in the $X$ mode is $n_{e0} \cong 2.3 \times 10^{19}\,m^{-3}$.

## 1 Electron Cyclotron Emission

The radiation resulting from the movement of the electrons around the magnetic field lines carries valuable information about the distribution function of the electrons in a plasma and its detection constitutes an important diagnostic method for magnetic confined plasmas [ 1 ]. In tokamak machines, the radial dependence of the magnetic field allows the determination, from the ECE radiation, of the electron temperature and also, in some situations, of the electron density [ 2 ].

The first work on the use of the ECE radiation, as a diagnostic tool, in tokamaks was published in 1974 [ 3 ]. Today, besides being an obligatory diagnosis technique in tokamaks for electron temperature measurements, it is in continuous evolution and, more recently, it has been used experimentally with more elaborated purposes, for instance, in the characterization of electron distribution of non-thermal electrons [ 4 ], in the transport studies involving temperature fluctuations [ 5 ] and, in recent proposals, involving Bernstein waves for the determination of electron temperature [ 6 ]. The use of the Bernstein waves seems to be particularly interesting in spherical tokamaks where the accessibility and the absorption conditions are not satisfied for the radiation used in common machines.

For a tokamak of major radius $R_0$ and toroidal field $B_{T0}$ , the harmonic $n$ of the ECE frequency $f_n$ emitted at radius $r$ , in the equatorial plane, is given by

$$f_n = \frac{n\,e\,B_{T0}\,R_0}{2\,\pi\,m_e\,\gamma\,(\,R_0 + r\,)}\,,$$

where $e$ and $m_e$ are respectively the electron charge and mass. The relativistic factor $\gamma$ , for the usual temperatures found in tokamaks like TCABR, can be considered as unity.

The transport of the electron cyclotron radiation in a thermal plasma is given by

$$I\,(\omega) = I_B\,(\omega)\,(\,1 - e^{-\tau(\omega)}\,),$$

where $I(\omega)$, the intensity of radiation, is the radiative power per unit area per unit solid angle per unit of angular frequency, $\tau(\omega)$ is the optical depth given by

$$\tau\,(\omega) = -\int_L^0 \alpha(\omega)\,ds\,,$$

$\alpha(\omega)$ is the absorption coefficient and $I_B(\omega)$ is the Rayleigh-Jeans approximation for the blackbody radiation given by $I_B(\omega) = \omega^2 k T_e/8\pi^3 c^2$. For an optically thick plasma ( $\tau(\omega) > 1$ ) substantial absorption occurs and results

$$I\,(\omega) = I_B\,(\omega) = \frac{\omega^2\,k\,T_e}{8\,\pi^3\,c^2}\,.$$

Therefore, for a given frequency, the detected radiative power is proportional to the electron temperature.

*Instituto Astronômico e Geofísico, USP

TABLE 1. First three harmonics of the ECE radiation ( in $GHz$ ) for the TCABR. $R_0$ - center of the plasma column, $R_{max}$ - external plasma edge, $R_{min}$ - internal plasma edge.

| | $R\,(cm)$ | $B\,(T)$ | $f_1\,(GHz)$ | $f_2\,(GHz)$ | $f_3\,(GHz)$ |
|---|---|---|---|---|---|
| $R_{max}$ | 79.5 | 0.93 | 25.9 | 51.8 | 77.7 |
| $R_0$ | 61.5 | 1.20 | 33.5 | 67.0 | 100.5 |
| $R_{min}$ | 43.5 | 1.70 | 47.4 | 94.9 | 142.3 |

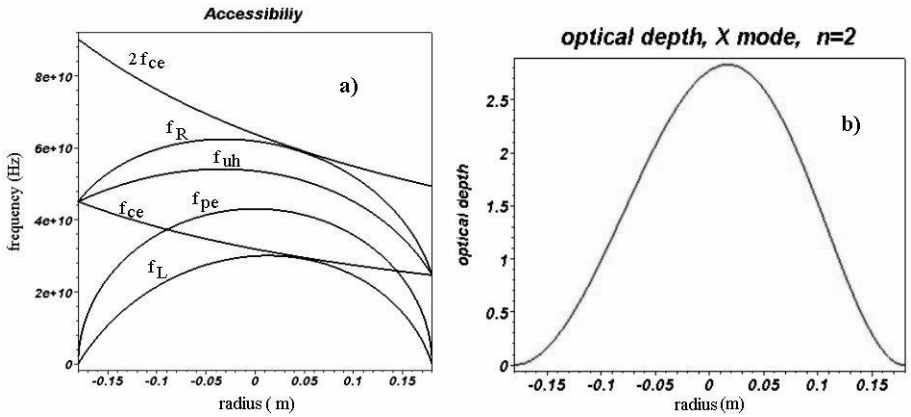


Figure 1. **a.** Radial profiles of : first ( $f_{ce}$ ) and second ( $2f_{ce}$ ) of the ECE radiation, $f_R$ - right-hand cutoff frequency, $f_{uh}$ - upper hybrid resonance frequency, $f_L$ - left-hand cutoff frequency and $f_{pe}$ - electron plasma frequency. $B_0 = 1.14\,T$, $n_{e0} = 2.3 \times 10^{19} m^{-3}$ and $T_{e0} = 500\,eV$. **b.** Radial profile of the optical depth for the second harmonic extraordinary mode for $B_{T0} = 1.14\,T$, $n_{e0} = 2.3 \times 10^{19} m^{-3}$ and $T_{e0} = 500\,eV$.

# 2 Electron Cyclotron Emission in the TCABR

The main parameters of the TCABR [7] are : major radius $R_0 = 61.5\,cm$ ; plasma radius $a = 18\,cm$ ; toroidal magnetic field ( maximum value ) $B_{T0} = 1.2\,T$ ; electron density $n_e = 2.5 \times 10^{19}\,m^{-3}$ and peak electron temperature $T_{e0} = 500\,eV$ . In the equatorial plane we have $r_{min} = 43.5$ cm and $r_{max} = 79.5\,cm$ . For these conditions, the frequencies of the first three harmonics of ECE are given in the Table 1.

As it will be discussed below, for the TCABR, the ECE radiation accessibility and absorption conditions indicate that the second harmonic extraordinary wave can be used as a diagnostic tool.

## 2.1 Accessibility and absorption conditions

The accessibility conditions can be discussed examining the Fig. 1.a. In this figure we see the radial profiles of the following frequencies : the first and the second harmonics of the electron cyclotron frequency

$$f_{ce} = \frac{e\,R_0\,B_{T0}}{2\,\pi\,m_e\,(R_0 + r)};$$

the right and left-hand cutoff frequencies

$$f_{R,L} = \frac{f_{ce}}{2}\,[\pm 1 + (1 + \frac{4\,f_{pe}^2}{f_{ce}^2})^{\frac{1}{2}}];$$

the upper-hybrid resonance frequency $f_{uh} = (f_{ce}^2 + f_{pe}^2)^{\frac{1}{2}}$ and the plasma frequency

$$f_{pe} = \frac{1}{2\,\pi}\,(\frac{n_o\,e^2}{\epsilon_o\,m_e})^{\frac{1}{2}}\,.$$

To discuss absorption conditions of the plasma, the most important parameter is the optical depth $\tau(\omega)$. In the Fig. 1.b the optical depth radial profile for the TCABR is shown. For the extraordinary mode ( $n \geq 2$ ) and perpendicular propagation ( $\theta = \pi/2$ ) parallel to the equatorial plane of the torus $\tau(\omega)$ is given by [ 8 ] :

$$\tau_n^{(X)} = \tau_n^{(X)}\,(\theta = \frac{\pi}{2}) = \frac{\pi^2\,n^{2(n-1)}}{2^{n-1}\,(n-1)!}\,(\frac{f_{pe}}{f_{ce}})^2\,(\frac{\nu_t}{c})^{2(n-1)}\,\mu_n^{(X)}(\theta = \frac{\pi}{2})\,(\frac{R_0}{\lambda_0})\,,$$

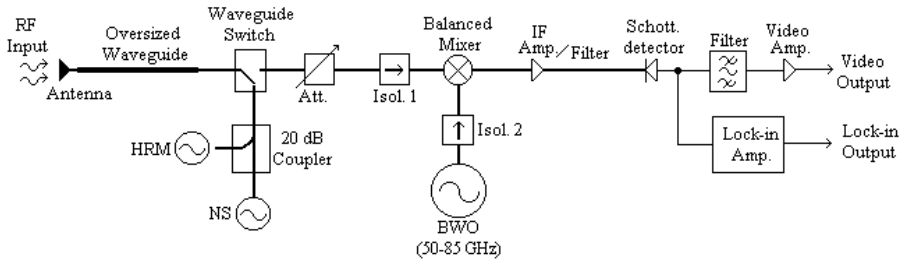


Figure 2. Block diagram of the TCABR heterodyne radiometer for the detection of X-mode second harmonic electrocyclotron radiation.

where

$$\mu_n^{(X)}(\theta = \frac{\pi}{2}) \cong 1 - (\frac{n - \frac{3}{2} - \frac{2}{n}}{n^2 - 1})(\frac{f_{pe}}{f_{ce}})^2,$$

$\nu_t = \sqrt{kT_e/m_e}$ and $\lambda_0 = c/f_c$.

To construct the curves shown in Fig. 1.a and Fig. 1.b we assumed parabolic profiles for the electron density and temperature. Those profiles are simple and easy to use and represent quite well most of observed experimental data. The profiles used to obtain Fig. 1 were :

$$n_e(r) = n_{e0}\,[1 - (\frac{r}{a})^{\xi}]^{\beta},\ \ T_e(r) = T_{e0}\,[1 - (\frac{r}{a})^{g}]^{\delta},$$

where $\xi = 2, \beta = 1, g = 2$ and $\delta = 1$. In those profiles, $a$ is the plasma radius, $n_{e0}$ is the peak electron density and $T_{e0}$ is the peak electron temperature. For those curves $B_{T0} = 1.14\,T$, $n_{e0} = 2.3 \times 10^{19}\,m^{-3}$ and $T_{e0} = 500\,eV$.

The ECE radiation in the *O-mode n=1* is inacessible since $f_{pe} > f_{ce}$, as can be seen in Fig. 1.a. For the *O-mode n=2* the plasma is optically thin ($\tau \sim 10^{-3}$). For the *X-mode n=1*, the radiation is inacessible since, if the antenna is in the low field side of the machine, the ECE radiation will be cutoff when it run into the $f_{uh} < f < f_R$ region. For $n > 2$ the plasma is optically thin for both modes and, the use of ECE radiation for diagnostic purposes becomes difficult. For the TCABR, it is more suitable the use of the *X-mode n=2* ECE radiation. Considering that the TCABR has low toroidal magnetic field ($B_{T0} \leq 1.2\,T$), we need to work in plasma scenarios with densities lower than $2.3 \times 10^{19} m^{-3}$ to access all the ECE radiation. In spite of the limitations relating the TCABR accessibility and absorption conditions, that are typical in medium and small tokamak machines, it is possible the measurement of the electron temperature in most relevant plasma scenarios.

# 3 The TCABR heterodyne sweeping radiometer

For the detection of the ECE radiation in TCABR a heterodyne sweeping radiometer [9], operating in the frequency range $52\,GHz < f < 85\,GHz$ was developed. This range allows the detection of the ECE radiation of 3/4 of the plasma column. In the Fig. 2 the block diagram of the radiometer is shown.

The microwave signal coming from the antenna goes to the mixer and then to the IF filter/amplifier. After that, we have the difference between the signal $f_s$ and the local oscillator $f_{LO}$ frequencies. The $\mid f_s - f_{LO} \mid$ signal is demodulated ( video detector ) and amplified ( video amplifier ). The video amplifier output signal goes to the data acquisition system where is digitalized and stored for later data analysis.

The local oscillator is a BWO ( Backward Wave Oscillator ) that is basically a voltage controlled oscillator. The control voltage ( variable from 2.2 to $8.5\,V$ and generated by a Digital to Analog Converter ) determines the detected frequency. That frequency keeps a direct relationship with the plasma position ( for plasmas that are not very hot ).

The system can operate in measurement or calibration mode. In measurement mode, the plasma signal is coupled to the mixer by a mechanical switch. In the calibration mode, the mixer is coupled to a harmonic oscillator, operating in 54, 60, 66, 72, 78 and $84\,GHz$ used for frequency calibration, or to a noise generator used for amplitude calibration check. A mechanical waveguide switch and a $20\,dB$ directional coupler are used to commute the radiometer from the measurement mode ( coupled to the plasma ) to the calibration mode.

The calibration in amplitude ( intensity ) can be made or checked in three ways : by direct calibration using a blackbody emitter with a known temperature, by the use of a cryogenic matched load immersed in liquid nitrogen or at the room temperature or, finally, we can use a noise source to check the calibration. The first way is the best one but is difficult and takes a longer time. The last way can be used as an easy way to check the calibration.

The TCABR radiometer main parameters are : Frequency range 52 - $85\,GHz$; BWO output power 4 - $20\,mW$ ; LO sweep time ( from 52 to $85\,GHz$ ) $150\,\mu s$; Minimal time for one LO frequency step $50\,\mu s$; Noise temperature $< 13\,dB$; IF ( amplifier/filter ) frequency band $0.1 - 1\,GHZ$; Harmonic Oscillator frequencies: $54, 60, 66, 72, 78, 84\,GHz$ ; Noise Source ENR ( Equivalent Noise Ratio ) $15\,dB$; NS stability $0.01\,dB/^oC$; NS Flatness $\pm 1.5\,dB$. The radiometer is a double-sideband receiver ( DSB ) since it is sensitive to both sideband frequencies. In the calculation of the horizontal space resolution, a $2\,GHz$ frequency band was used.

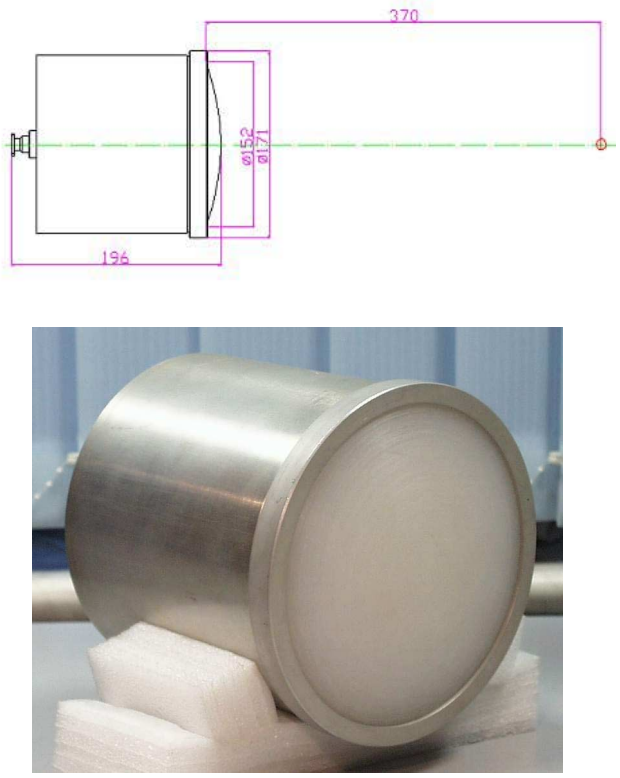


Figure 3. Gaussian antenna used for the ECE detection in TCABR tokamak. **a.** Antenna dimensions in $mm$. **b.** Photo of the antenna.

A Gaussian antenna, used for better spatial resolution, makes the coupling of the radiometer with TCABR plasma. In Fig. 3 a diagram and a photo of the antenna are shown. The waist of the beam at the antenna focus ( $\cong 2\,cm$ ) defines the vertical space resolution for the ECE detection. The total ECE spatial resolution ( vertical and horizontal ) is about $2\,cm$. The radiometer is placed $5\,m$ away from the tokamak and an oversized waveguide is used to reduce the losses.

# 4 Experimental results

## 4.1 Sensibility and absolute calibration

The radiometer sensibility is related to the minimum level of the power that can be measured. This is related with the intrinsic thermal noise associated to the instrument. An important parameter that defines the sensibility of the radiometer is its noise figure *F = (input signal to noise ratio)/(output signal to noise ratio).* In ECE detection, the signal in the antenna input is of the order of $nW$. The thermal noise power in the input of the radiometer that have a frequency band $B$, with the antenna coupled to a blackbody of temperature $T$ is given by $P = kTB$. Here the Rayleigh-Jeans approximation ( $hf \ll kT$ ) was used. The radiometer noise figure is given by

$$F = \frac{P_{si}/kTB}{AP_{si}/(AkTB + P_{nA})} = 1 + \frac{P_{nA}}{AkTB},$$

where $P_{si}$ is the input signal power, $A$ is the radiometer power gain and $P_{nA}$ the output noise power ( internal power ). Note that $AkTB + P_{nA}$ is the total noise power at the radiometer output. Normally we adopt $T = T_0 = 290\,K\,(17^oC)$. From the above relation the noise power generated by the radiometer is given by

$$P_{nA} = A\,k\,T_0\,B\,(F - 1).$$

It is also possible describe the noise properties of the radiometer using the noise temperature $T_n$. Taking $P_{nA} = AkT_nB$, $T_n$ is given by

$$T_n = (F - 1)\,T_0.$$

The measurement of the noise figure of the TCABR radiometer was made by the two temperatures method ( or Y factor method ). In this method, two emitters with two different temperatures : hot $T_h$ ( $\approx 300\,K$ ) and cold $T_c$ ( $77\,K$ ) are used. We define $Y$ factor as the ratio of the radiometer output power when the hot and the cold bodies are placed in front of the antenna :

$$Y = \frac{P_h}{P_c} = \frac{k(T_n + T_h)\,B}{k(T_n + T_c)\,B} = \frac{T_n + T_h}{T_n + T_c}$$

or

$$T_n = \frac{T_h - Y\,T_c}{Y - 1}.$$

Using the above expressions we obtain the noise figure $F_{dB} = 10\,[\,log_{10}\,(\,1 + T_n/T_0\,)]$.

Another useful parameter is the *Equivalent Noise Ratio - ENR* that keeps a direct relationship with the noise temperature $T_n$, and is defined by $ENR = 10\,log\,[\,T_n/(T_0 - 1)\,]$.

To measure $T_n$ and the noise figure we used a matched load, shown in Fig. 4.a, that was used in liquid nitrogen and also at room temperature. The matched load ( microwave absorber ) was coupled to the radiometer input. In Fig. 4.b we show the noise temperature and the noise figure for all the radiometer frequency bandwidth.

Besides the Noise Temperature $T_n$ and Noise Figure $F$, it is important to obtain experimentally a calibration curve relating the radiometer output signal ( in *volts* ) with the temperature ( in $eV$ ) [10]. In this calibration, we used the experimental arrangement shown in Fig. 5. For the calibration, we used two thermal sources with two different temperatures ( $T_h$ and $T_c$ ). In this measurement, the distances involving the emitter, antenna and the radiometer were the same as those when the radiometer was coupled to the TCABR machine. In the corresponding position where the center of the plasma column would be, we put two emitters one in high temperature and the other in low temperature.

In Fig. 6.a. we show the output signal ( in function of frequency ) of the radiometer for emitters in the high temperature $T_h$ ( $923\,K = 650^oC$ ) and low temperature $T_c$ ( $77\,K$ ). In the Fig. 6.b, the frequency dependence of the difference of the two signals is shown for five measurements. From these measurements, we obtain the calibration curve shown in Fig. 7.

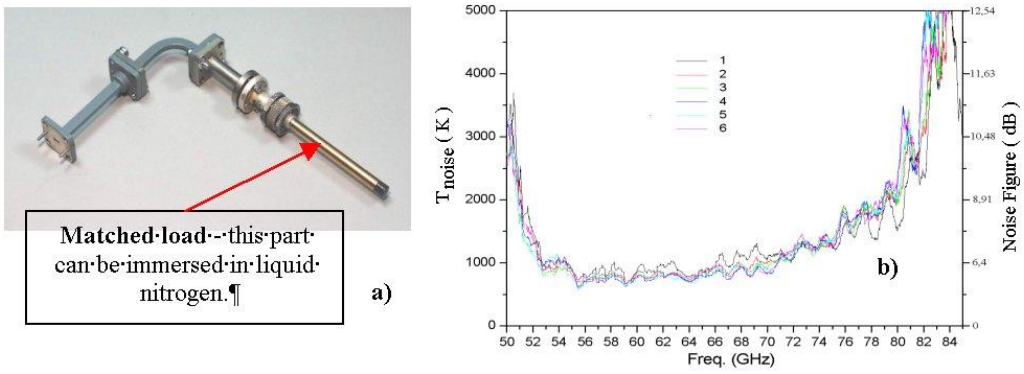


Figure 4. **a.** Matched load used for noise temperature measurements. **b.** Noise temperature $T_n$ and noise figure $F_{dB}$ for the TCABR radiometer for six measurement.

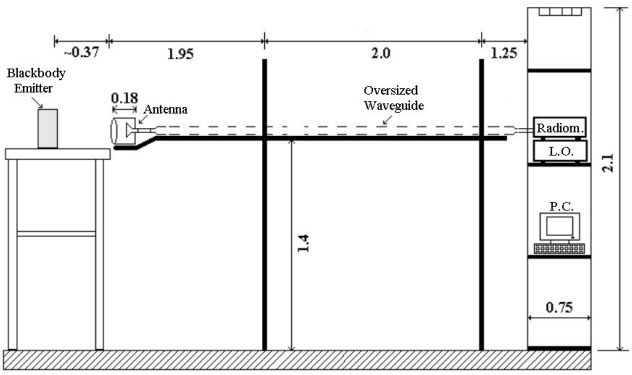


Figure 5. Experimental apparatus used for the radiometer absolute calibration. Dimensions in meters.

To obtain the final absolute calibration curve, the absorption and reflection characteristics of the diagnostic glass window were measured [11] in the frequency range of the radiometer. The radiation coming from the plasma is partially reflected and also partially absorbed by the glass. The measurement was done with two thermal sources ( hot and cold ) and applying, for each case, the radiation transport equation [12] :

$$I_{h2} \;=\; I_{h1}\, e^{-\tau}\,(1-r)^2 \;+\; I_{T_{amb}}\,(1-e^{-\tau})\,(1-r)$$

and

$$I_{c2} \;=\; I_{c1}\, e^{-\tau}\,(1-r)^2 \;+\; I_{T_{amb}}\,(1-e^{-\tau})\,(1-r)$$

From these equations, we obtain

$$e^{-\tau}\,(\,1\,-\,r\,)^2 \;=\; \frac{I_{h2}\,-\,I_{c2}}{I_{h1}\,-\,I_{c1}}\,,$$

where $I_{h1}$ and $I_{c1}$ are the radiative intensities attaining the glass window coming from the hot and cold sources, $I_{T_{amb}}$ is the radiative intensity emitted by the glass, $I_{h2}$ and $I_{c2}$ are the radiative intensities from the hot and cold sources after passing through the glass window, $\tau$ is the optical depth of the glass and $r \;=\; [(n-1)/(n+1)]^2$ is the glass reflection coefficient. In the Fig. 8 the final calibration curve is shown. This curve was obtained multiplying the curve of Fig. 7 by the factor $e^{-\tau}\,(\,1\,-\,r\,)^2$ . The error bars shown in the figures were obtained from five different measurements of the calibration curve.

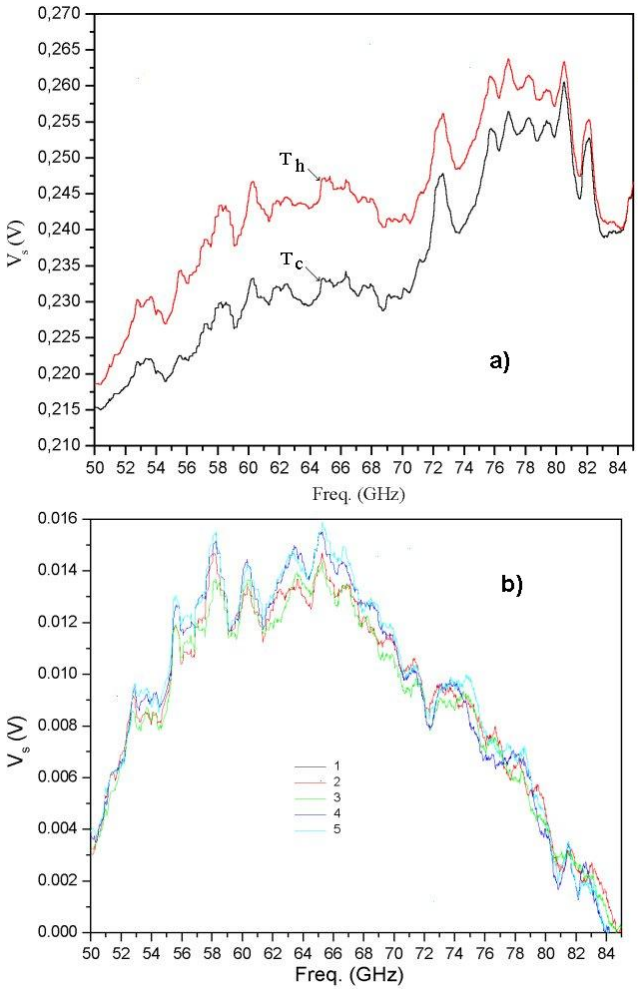


Figure 6. **a.** Radiometer output signal ( in *volts* ) in function of frequency ( in $GHz$ ), for the cold emitter ( 77 $K$ ) and the hot emitter ( 923 $K$ ). **b.** Difference of the two signals in function of the frequency for 5 measurements.

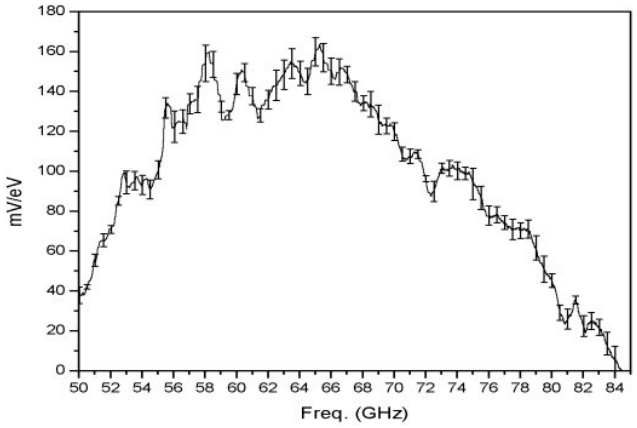


Figure 7. Absolute calibration curve ( $mV/eV$ ) obtained from the curves of the Fig. 6.b.

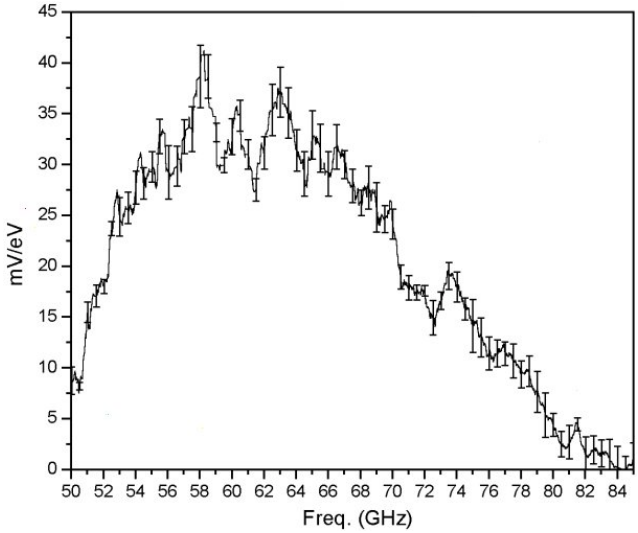


Figure 8. Final calibration curve.

The absolute calibration of the radiometer takes a lot of work and time to be done. The calibration curve depends on the characteristics of the radiometer components, particularly of the BWO, that may change with time. For this reason, the calibration curve should be checked routinely. This checking is easily done, at the begining of each tokamak session, using the noise generator and the harmonic oscillator.

### 4.2 Time and radial profiles of the plasma temperatures

Finally, we show radial and temporal profiles of the electron temperature obtained with the radiometer. These results illustrate measurements made with the radiometer in the two modes of operation : sweeping ( several radial positions ) and fixed frequency ( high time resolution ). Results of ECE radiation detection in a high-density plasma scenario ( above the cutoff frequency ) are also shown.

In Fig. 9, seven temporal profiles are presented for the radial positions : $+12.6\,cm, +8.5\,cm, +3.5\,cm, +1.3\,cm, -4.5\,cm, -7.8\,cm, -12.1\,cm$ . In that pulse the plasma density is lower than the right-hand cutoff density ( $n_e < 2.3 \times 10^{19}\,m^{-3}$ ). We verify that in the initial stage of the discharge ( $0 < t < 15\,ms$ ) the intensity of the ECE radiation is relatively high due the occurence of suprathermal electrons that appear during the rising phase of the plasma density. These electrons are accelerated by the toroidal electric field present in the breakdown and heating phases of the discharge. After the initial stage of the discharge, there is a time interval ( $15 < t < 95\,ms$ ) where we have a thermal plasma and the detected ECE radiation has a lower time variation. In the Fig. 9.b a radial profile of $T_e$ , for $t = 50\,ms$ , is shown, where the peak electron temperature is $\approx 500\,eV$ .

In Fig. 10, temporal and radial profiles of ECE emission are shown in a 3D plot for a discharge where the electron density is higher than the right-hand cutoff ( $n_e > 2.3 \times 10^{19}\,m^{-3}$ ). This pulse has duration of about $100\,ms$ . We verify that, for the interval between 30 and 70 $ms$ , there is a decrease of the radiation intensity due to the increase of the plasma electron density that becomes higher than the cutoff density. This behavior of the detected ECE radiation can be used to obtain information on the radial electron density profile [13].

Finally we show results [14] obtained with the radiometer in the fixed frequency mode. In this mode, the radiometer time resolution is $10\,\mu s$ . In Fig. 11, 15 ECE time profiles of the electron temperature are shown. To obtain those profiles, 15 tokamak shots were used. Care was taken to use only very reproducible shots and we used one shot for each profile. For each shot, the frequency of the local oscillator was changed allowing the measurement of the electron temperature for different radial position between $r = -4\,cm$ and $r = +14\,cm$ . In these profiles, it is possible to see clearly the occurrence of sawteeth oscillations. It is observed that, in the radial position $r \cong +4\,cm$ , we have the inversion of the sawtooth. In this radius the safety factor is unitary ( $q = 1$ ). Internally to the surface $q = 1$ ( $-4\,cm < r < +4\,cm$ ) a slow growth of the electron temperature is followed by an abrupt fall, and externally to that surface we have an opposite behavior, an abrupt increase of the temperature is followed by a slow fall. The duration of the sawteeth is about $400\,\mu s$ .

## 5 Conclusions

It was coupled, with success, in the TCABR tokamak, a heterodyne radiometer that operates in the 52 to 85 $GHz$ frequency range. The radiometer noise figure was measured and the value obtained was $F_{dB} \cong 12\,dB$ . The noise temperature is about $3000\,K$ . The absolute calibration curve, for the entire frequency band, was obtained and the sensibility of the radiometer, for $60\,GHz$ , is $\cong 35\,mV/eV$ . The radiometer is in operation in TCABR and detects the ECE radiation for the second harmonic X-mode. Regularly, for thermal plasmas, the radiometer is used to obtain time and

radial profiles of plasma temperature. For non-thermal plasmas, particularly those with runway electrons, a large increase in the ECE radiation is observed. For a magnetic field of $B_{T0} = 1.14\,T$ it was verified that we can access the ECE radiation up to a density of $n_e = 2.3 \times 10^{19}\,m^{-3}$ where the right-hand cutoff occurs.

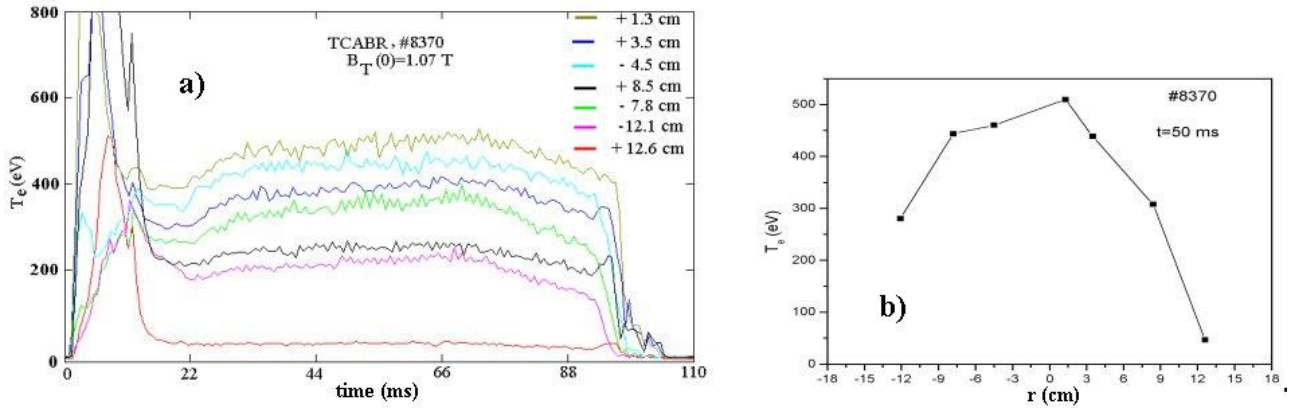


Figure 9. **a.** Time profiles of the electron temperature obtained in TCABR. The radiometer was in sweeping mode. The calibration curve shown in Fig. 8 was used to obtain the temperature. Seven time profiles are shown for the following radial positions : $+12.6\,cm$, $+8.5\,cm$, $+3.5\,cm$, $+1.3\,cm$, $-4.5\,cm$, $-7.8\,cm$, $-12.1\,cm$. For this discharge the toroidal field was $B_{T0} = 1.07\,T$. **b.** Radial profile for the same pulse obtained for $t = 50\,ms$. The peak temperature is about $500\,eV$.

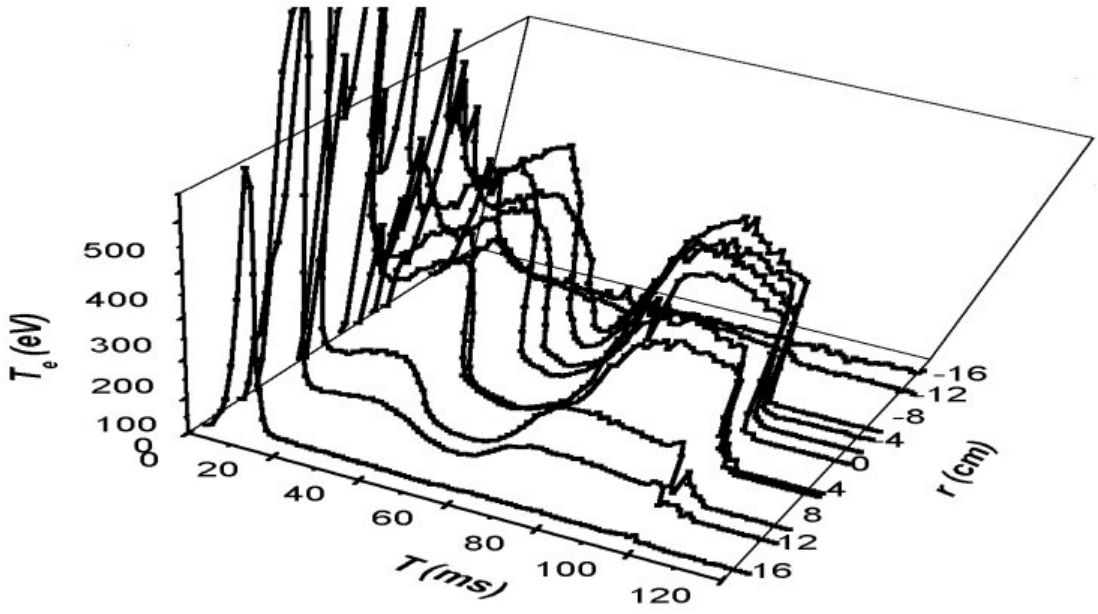


Figure 10. Time and radial profiles for the electron temperature ( 3D plot ) obtained in the TCABR. In this discharge, the density is higher than the cutoff and we can observe a reduction in the detected ECE radiation [13] between 40 and $50\,ms$.

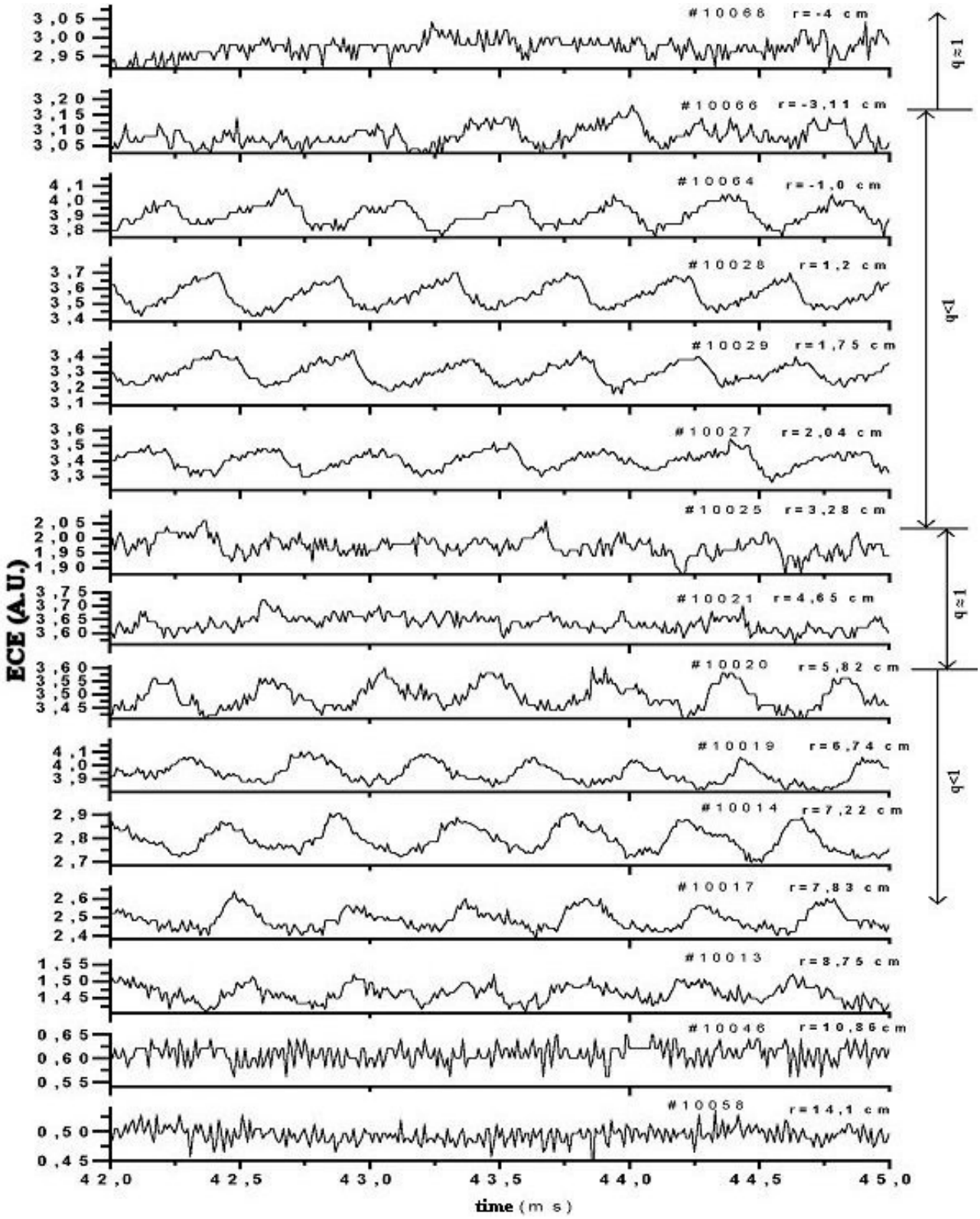


Figure 11. Time profiles obtained in the TCABR with the radiometer working in fixed frequency mode ( time resolution of $10\,\mu s$ ) for 15 different radial positions from $r = +14.1\,cm$ ( internal ) to $r = -4.0\,cm$ ( external ). The toroidal field in the column center is $1.13\,T$. The electron density is $1.2 \times 10^{19}\,m^{-3}$. It is possible to observe sawteeth oscillations.

**Acknowledgements**

This work was partially supported by the Fundação de Amparo à Pesquisa do Estado de São Paulo ( FAPESP ).

# References

[1] M. Bornatici, R. Cano, O. De Barbieri, and F. Engelman, Nuclear Fusion, **23**, 1153 (1983).

[2] D. A. Boyd, Intern. Journal of Infrared and Millimeter Waves, **1**, 45 (1980).

[3] A. E. Costley, R. J. Hastie, J. W. M. Paul, and J. Chamberlain, Phys. Rev. Lett. **33**, 758 (1974).

[4] M. Brusati, D. V. Bartlett, A. Ekedahl, P. Froissard, A. Airoldi, G. Ramponi, R. P. da Silva, and Y. Peysson, Nuclear Fusion **34**, 23 (1994).

[5] J. W. Heard, C. Watts, R. F. Gandy, P. E. Phillips, G. Cima, R. Chatterjee, A. Blair, A. Hubbard, C. W. Domier, and N. C. Luhmann Jr, Rev. Sci. Instrum. **70**, 1011 (1999).

[6] P. C. Efthimion, J. C. Hosea, R. Kaita, R. Majeski, and G. Taylor, Rev. Sci. Instrum. **70**, 1018 (1999).

[7] I. C. Nascimento, R. M. O. Galvão, E. K. Sanada, Yu. K. Kuznetsov, A. P. Reis, F. T. Degasperi, N. A. M. Cuevas, J. I. Elizondo, A. G. Tuszel, R. P. da Silva, D. Campos, W. P. Sá, J. H. Vuolo, A. Vanucci, A. M. M. Fonseca, L. Ruchko, N. R. Nunes, V. S. W. Vuolo, and M. V. A. P. Heller, "Preliminary Results from the TCABR Tokamak", IAEA Technical Committee Meeting on Research Using Small Fusion Devices, 18-20 October 1999, F1-TC-536.15, Southwestern Institute of Physics Chengdu, China.

[8] M. Bornatici, F. Engelman, S. Novak, and V. Petrillo, Plasma Physics **23**, 1127 (1981).

[9] H. J. Hartfuss, T. Geist, and M. Hirsch, Plasma Phys. Control. Fusion **39**, 1693 (1997).

[10] P. F. Goldsmith, R. A. Kot, and R. S. Iwasaki, Rev. Sci. Instrum. **50**, 1120 (1979).

[11] A. M. M. Fonseca, R. P. da Silva, J. H. Vuolo, R. M. O. Galvão, and J. Raffaelli, "An experimental method for the optical characterization of materials at millimeter range", *X Latin American Workshop on Plasma Physics - 7th Brazilian Meeting on Plasma Physics*, Nov. 30 - Dec. 5, 2003, São Pedro, SP, Brazil.

[12] G. Bekefi, *Radiation Process in Plasmas*, Wiley, New York (1966).

[13] A. M. M. Fonseca, R. P. da Silva, R. M. O. Galvão Yu. K. Kuznetsov, J. I. Elizondo, L. F. Ruchko, and J. H. Vuolo, *"Electron Density Measurements from Right-Hand Cutoff of ECE in the TCABR Tokamak"*, to be published in Braz. J. of Phys. (2004).

[14] A. M. M. Fonseca, R. P. da Silva, J. H. Vuolo, R. M. O. Galvão, Yu. K. Kuznetsov, E. R. Calderon, and J. Raffaelli, *"Electron Cyclotron Emission from Thermal and Non-Thermal Discharges in the TCABR tokamak"*, 30th EPS Conference on Contr. Fusion and Plasma Phys., 7 - 11 July, St Petersburg ECA Vol. 27A, P-1.80, 2003.